Iranian Journal of Pharmaceutical Sciences
2026: 22 (1): 249-258
https://journals.sbmu.ac.ir/IJPS

Research Article

# Synthesis, characterization, and antibacterial evaluation of silver oxide nanoparticles (AgONPs) using terephthalic acid

Mohammad Talib al Alawi[a], Ali Talib al Alawi[a], Mobina Malaeke[b], Nasim Hayati Roodbari[a], Ali Es-haghi[b]*, Ehsan Yousefi[c]

[a] *Department of Biology, SR.C, Islamic Azad University, Tehran, Iran.*
[b] *Department of Biology, Ma.C., Islamic Azad University, Mashhad, Iran.*
[c] *Department of Cell and Molecular Biology, Faculty of Science, Isfahan University, Isfahan, Iran.*

**Received:** January 19, 2025 **Last Revision:** December 9, 2025 **Accepted:** May 3, 2026 **Available online:** August 02,2026.

**Abstract**

Recently, silver oxide nanoparticles (AgONPs) have come into the spotlight as promising options for cancer treatment. Their popularity stems primarily from their unique physical and chemical properties and their potential as effective anticancer agents. This study examines how these nanoparticles are made from terephthalic acid and then calcined at 600°C. After they are created, these nanoparticles are carefully examined to determine how they exhibit antibacterial activity. To fully understand these nanoparticles, several advanced analytical techniques are being used. These methods include X-ray Diffraction (XRD), Field Emission Scanning Electron Microscopy (FESEM), Fourier Transform Infrared Spectroscopy (FTIR), Dynamic Light Scattering (DLS), and zeta potential analysis. The results show that the AgONPs are mostly cubic, with an average size of 171.34 nm and a slightly negative zeta potential. Lab tests suggest that these nanoparticles exhibit strong antibacterial activity against Gram-negative and Gram-positive bacteria.

*Keywords*: Silver oxide nanoparticles; Antibacterial; Calcination.

## 1. Introduction

In recent years, the nanostructure constituents have received considerable attention from researchers due to their attractive properties and numerous industrial uses [1-6]. Among the nanoparticles (NPs), silver and silver oxide nanoparticles (AgONPs) have garnered significant attention in recent years due to their unique physicochemical properties and potential applications in various fields, including medicine [7-10]. Among these applications, the use of AgONPs in antibacterial and cancer treatment has emerged as a promising area of research [11-13]. Silver nanoparticles are interesting mainly because of their natural antimicrobial and anticancer properties, which help them induce oxidative stress in bacterial cells [14-16]. This makes them ideal for developing new therapeutic approaches [17-19]. This study focuses on the creation, characterization, and potential uses of AgONPs in microbial treatment, with a specific focus on their antibacterial effects against pathogenic bacteria. AgONPs are usually made through

*** Corresponding Authors**:
**Ali Es-haghi**, Department of Biology, Ma.C., Islamic Azad University, Mashhad, Iran. E-mail: ashaghi@gmail.com.

**Cite this article as**: al Alawi M.T., al Alawi A.T., Malaeke M., Hayati Roodbari N., Es-haghi A., Ehsan Yousefi E. Synthesis, characterization, and antibacterial evaluation of silver oxide nanoparticles (AgONPs) using terephthalic acid. Iran. J. Pharm. Sci., 2026, 22 (1): 249-258.

DOI: https://doi.org/10.22037/ijps.v22i1.47332

reducing silver ions in the presence of a stabilizing agent, which controls the size and shape of the nanoparticles [20]. For example, one environmentally friendly method involves using Rhynchosia capitata extract as both a reducing and stabilizing agent. The synthesized nanoparticles, averaging 21.66 nm in size, demonstrated significant antioxidant, antibacterial, and antifungal activities. This study highlighted the potential of synthesized AgONPs as cost-effective and bioactive agents for medical applications. The application of AgONPs in antimicrobial applications primarily relies on their ability to induce oxidative stress in bacterial cells [21-24]. Oxidative stress is caused by the generation of reactive oxygen species (ROS), which can damage cellular components such as DNA, proteins, and lipids [25-28]. Their ability to induce oxidative stress in bacterial cells, coupled with their potential to enhance conventional cancer therapies, highlights their therapeutic potential. Further research is needed to understand the mechanisms underlying their antibacterial activity fully and to develop safe and effective AgONP-based treatments. This study adds to the growing body of knowledge on AgONPs in microbial treatment and lays the foundation for future research in this field.

Understanding the bactericidal activity of AgONPs is important for assessing their potential use and safety in therapies. Making AgONPs from terephthalic acid and then calcining them at 600°C provides a controlled method for producing nanoparticles with specific properties. Advanced characterization methods like X-ray Diffraction (XRD), Field Emission Scanning Electron Microscopy (FESEM), Fourier Transform Infrared Spectroscopy (FTIR), Dynamic Light Scattering (DLS), and zeta potential analysis were used to closely examine the physical and chemical characteristics of the nanoparticles that were synthesized. The results of this study will enhance our understanding of AgONPs' antimicrobial activity and provide valuable insights into their potential as effective antibacterial agents.

## 1. Experimental methods

### *1.1. Synthesis and characterization of nanoparticles*

Silver oxide nanoparticles (AgONPs) were synthesized from terephthalic acid via calcination at 600°C. Initially, a silver nitrate solution was prepared by dissolving 1.0 g of silver nitrate in 50 mL of deionized water. Separately, 0.5 g of terephthalic acid was dissolved in 50 mL of ethanol. The terephthalic acid solution was then slowly added to the silver nitrate solution with continuous stirring for 2 hours at room temperature, resulting in the formation of a silver-terephthalate complex. The precipitate was filtered, washed with ethanol, and dried at 60°C for 12 hours to obtain the silver-terephthalate precursor. The dried precursor was placed in a ceramic crucible and calcined in a muffle furnace. The furnace was heated to 600°C at 10°C/min and maintained at this temperature for 3 hours to ensure complete calcination. After cooling to room temperature, the calcined product, consisting of silver oxide nanoparticles, was collected. The nanoparticles were characterized using various techniques, including X-ray Diffraction (XRD) to confirm their crystalline structure, Field Emission Scanning Electron Microscopy (FESEM) to observe their morphology, Fourier Transform Infrared Spectroscopy (FTIR) to identify functional groups, Dynamic Light Scattering (DLS) to measure size distribution, and zeta potential analysis to determine surface charge and stability.

### *1.2. Antibacterial activity of AgONPs*

Gram-positive [*Bacillus subtilis* (PTCC 1365) and *Staphylococcus aureus* ATCC 25923] and Gram-negative [*Escherichia coli* ATCC 25922 and *Pseudomonas aeruginosa* ATCC 9027] bacteria were used in antibacterial tests. These experiments were performed in 3 replicates. The disc diffusion method was used to evaluate antibacterial properties [29, 30].

A blank disk was prepared by loading it with AgONPs at a concentration of 100 µg/mL. A bacterial suspension with an $OD_{620}$ of 0.01 was uniformly spread on Muller-Hinton agar. The AgONP-loaded disks were then placed on the agar surface [31, 32]. The plates were incubated at 37°C for 24 hours. After incubation, the diameter of the bacterial inhibition zone was measured in millimeters. Gentamicin was used as a positive control to confirm antibiotic sensitivity, while a disk dipped in sterile distilled water served as a negative control.

### *2.3. Minimum inhibitory concentration and minimum bactericidal dose*

The microbroth dilution method was used to determine the minimum inhibitory concentration (MIC) and minimum bactericidal concentration (MBC) [31]. A 24-well microplate was utilized, with AgONPs prepared at concentrations of 0, 25, 50, 75, ..., up to 300 µg/ml. Chloramphenicol served as the control antibiotic. Bacteria were inoculated into each well with a standard concentration ($OD_{620}$ = 0.01), and the microplate was incubated at 37°C for 24 hours. The MIC was determined as the lowest concentration at which no bacterial growth was observed.

To determine the MBC, samples from wells without growth were inoculated onto nutrient agar plates (without nanoparticles) and incubated at 37°C for 24 hours. Colony formation on the plates indicated bacterial viability, while the absence of colonies indicated that the bacteria had been killed, identifying the MBC.

The MBC/MIC ratio was then calculated to assess antibacterial activity. If the ratio is ≤ 4, the agent is considered bactericidal; if the ratio is > 4, it is considered bacteriostatic [33].

### *2.4. Investigating the ability of biofilm formation*

The purpose of this experiment was to promote strong biofilm formation. The biofilm-forming ability of each bacterial strain was assessed using a modified microtiter plate method. Modifications included using distilled water for washing instead of phosphate-buffered saline (PBS) and extending the incubation time. In each well of a 96-well microplate, 180 µl of Tryptone Soy Broth (TSB) medium was added, followed by 10 µl of sterile distilled water. Then, 10 µl of pure bacterial suspension ($OD_{620}$ = 0.01) was added, bringing the total volume in each well to 200 µl. Wells in the first row, containing 200 µl of TSB without bacteria, served as negative controls (blanks).
The microplate was incubated at 37°C for 48 hours. After incubation, the contents of the wells were carefully discarded, and the wells were washed 3 times with distilled water. To fix the biofilm, 200 µl of 95% ethanol was added to each well for 15 minutes. For staining, 200 µl of 0.025% safranin was added to the wells for 10 minutes. After discarding the stain, the wells were washed several times with distilled water and allowed to dry. Finally, 200 µl of 33% glacial acetic acid was added to dissolve the stain, and after 15 minutes, the absorbance of the wells was measured using an ELISA reader at 492 nm.

The biofilm-forming ability of bacterial strains was assessed using the cut-off optical density (ODc) method. The ODc was calculated as the mean OD of the negative control plus 3 times its standard deviation. The measured OD for each strain was compared with ODc to determine biofilm-forming ability, using the formula and standard patterns provided in **Table 1**.

**Table 1.** Biofilm formation based on $OD_{492nm}$ measured in wells

| Biofilm production | Average OD |
|---|---|
| Negative biofilm | OD ≤ ODc |
| Weak biofilm | ODc < OD ≤ 2 × ODc |
| Medium biofilm | 2 × ODc < OD ≤ 4 × ODc |
| Strong biofilm | 4 × ODc < OD |

### *2.5. Assessment of the effect of AgONPs on biofilm formation*

The anti-biofilm effects of AgONPs were evaluated using a modified microtiter plate method. First, 180 µl of Tryptone Soy Broth (TSB) medium was added to all wells of a 96-well microplate. Then, 10 µL of the serial dilutions of silver oxide nanoparticles was added to each well. Finally, 10 µl of a pure bacterial suspension ($OD_{620}$ = 0.01) was inoculated into each well, bringing the total volume to 200 µl. The concentrations of silver oxide nanoparticles in the wells ranged from 0 to 300 µg/mL.

As controls, the wells in the first row contained 180 µl of TSB medium, 10 µl of bacterial suspension, and 10 µl of sterile distilled water. The blank wells contained only 200 µl of TSB medium without bacteria. After incubating the microplate at 37°C for 24 hours, the biofilms were fixed and stained following the same procedure as in the previous method.

The experiment was done in triplicate, and the optical absorbance readings were averaged. The average data were then compared to assess the anti-biofilm effects of the silver oxide nanoparticles.

### *2.6. Assessment of the effect of AgONPs on the formed biofilm*

To investigate the effect of AgONPs on preformed biofilms, 180 µl of Tryptone Soy Broth (TSB) medium and 10 µl of bacterial suspension (at a 0.5 McFarland

standard concentration) were added to all wells of a 96-well microplate. The microplate was incubated at 37°C for 24 hours to allow biofilm formation. Control wells were included in the setup.

After 24 hours, 10 µl of serial dilutions of AgONP suspensions were added to each well, achieving final concentrations of 0, 25, 50, 75, and 300 µg/ml. After a 3-hour incubation, the contents of the microplate were carefully drained, and the wells were washed three times with distilled water. The biofilms were fixed with ethanol and stained with safranin, following the same procedure as in previous methods.

The optical absorbance of the dye dissolved in acetic acid was measured using an ELISA reader at 492 nm. The percentage of biofilm destruction was then calculated using Equation 1.

Equation 1:

$[[OD_{492}$ positive control / $OD_{492}$ biocide] × 100] - 100 = percentage inhibition of biofilm formation

### *2.7. Statistical analysis*

Statistical analysis was performed using SPSS software version 21. The mean ± standard deviation was calculated using one-way ANOVA, and p-values less than 0.05 ($p < 0.05$) were considered statistically significant.

## 3. Results and Discussion

### *3.1. X-ray Diffraction (XRD)*

The X-ray Diffraction (XRD) analysis of silver oxide nanoparticles (AgONPs) provides detailed information about their crystallographic structure. The reference code 01-076-1489 corresponds to silver oxide (AgO), with a cubic crystal system and space group F-43m (space group number 216). The lattice parameters are a = 4.8160 Å, b = 4.8160 Å, and c = 4.8160 Å, with all angles (alpha, beta, gamma) being 90.0000°. The XRD peak list provided further insights into the crystallographic planes and their corresponding d-spacing and 2Theta values. The most intense peak, with 100% relative intensity, is observed at a 2Theta value of 32.167°, corresponding to the (111) plane with a d-spacing of 2.78052 Å. Other significant peaks include those at 37.313° (2Theta) for the (200) plane, 53.795° for the (220) plane, and 64.076° for the (311) plane. These peaks confirm the presence of silver oxide in the sample and match well with the reference data. The presence of these characteristic peaks and their relative intensities indicates the high crystallinity of the AgONPs. The slight variations in the measured and calculated densities, as well as the peak intensities, can be attributed to factors such as particle size, shape, and possible defects in the crystal lattice. Overall, the XRD analysis confirms the successful synthesis of highly crystalline cubic silver oxide nanoparticles (**Figure 1**).

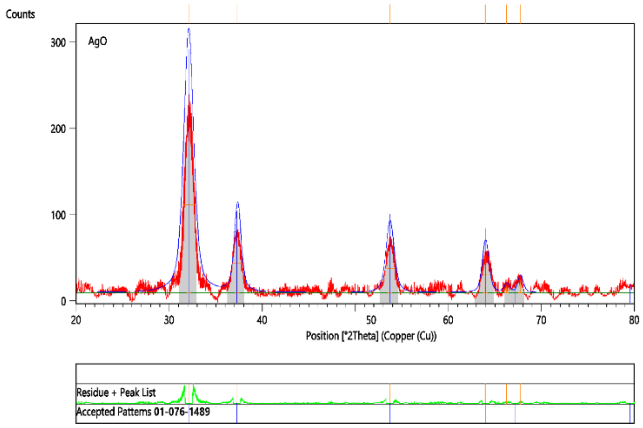


**Fig. 1:** XRD pattern of AgONPs with reference code 01-076-1489. The pattern confirms the cubic crystal system with space group F-43m, showing characteristic peaks at 2Theta values of 32.167°, 37.313°, 53.795°, 64.076°, and others, corresponding to various crystallographic planes.

### *3.2. Fourier Transform Infrared Spectroscopy (FTIR) analysis*

The FTIR analysis of AgONPs synthesized using terephthalic acid and calcined at 600°C revealed several characteristic absorption bands. The peaks at 426.81 $cm^{-1}$ and 481.84 $cm^{-1}$ are indicative of Ag-O stretching vibrations, confirming the presence of silver oxide in the sample. Additionally, the band at 560.74 $cm^{-1}$ corresponds to the bending vibrations of Ag-O bonds, further supporting the formation of silver oxide nanoparticles. The peak at 1060.24 $cm^{-1}$ is associated with C-O stretching vibrations, likely due to residual organic compounds from the terephthalic acid used in the synthesis process. Other significant peaks include 1424.65 $cm^{-1}$, which is characteristic of C=C stretching vibrations in aromatic rings, suggesting the presence of aromatic compounds from the terephthalic acid. The band at 1629.33 $cm^{-1}$

corresponds to C=O stretching vibrations, indicating the presence of carbonyl groups. The peak at 2918.28 $cm^{-1}$ is associated with C-H stretching vibrations in aliphatic compounds, suggesting the presence of hydrocarbon chains. Finally, the broad absorption band at 3443.90 $cm^{-1}$ is indicative of O-H stretching vibrations, which could be due to adsorbed water or hydroxyl groups on the surface of the nanoparticles. These FTIR results provide a comprehensive understanding of the chemical composition and functional groups of AgONPs (**Figure 2** and **3**).

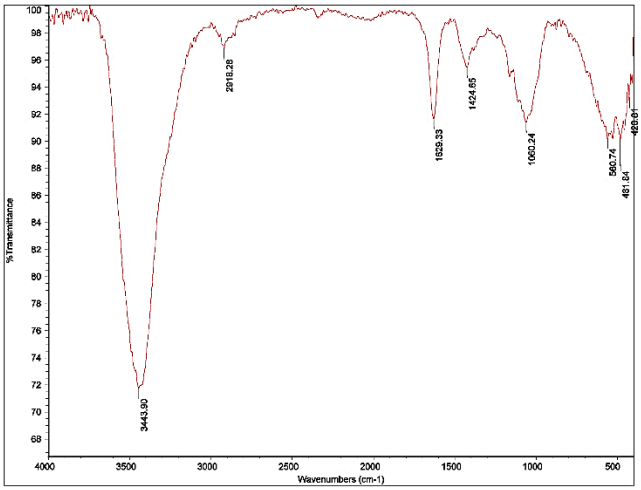


**Figure 2.** FTIR spectrum of AgONPs synthesized using terephthalic acid and calcined at 600°C. The spectrum shows characteristic absorption bands at 426.81 $cm^{-1}$, 481.84 $cm^{-1}$, 560.74 $cm^{-1}$, 1060.24 $cm^{-1}$, 1424.65 $cm^{-1}$, 1629.33 $cm^{-1}$, 2918.28 $cm^{-1}$, and 3443.90 $cm^{-1}$, indicating the presence of Ag-O bonds and various functional groups.

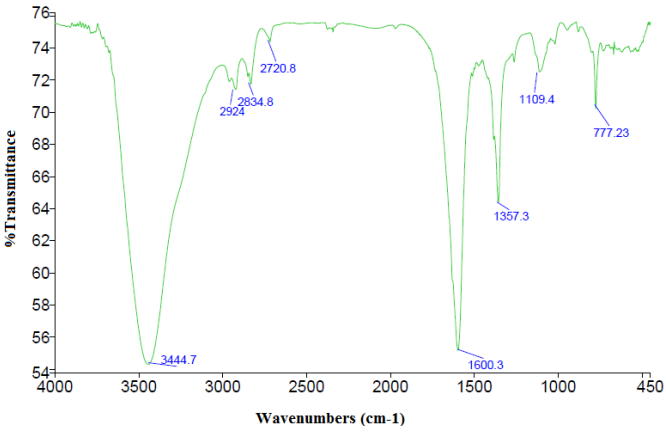


**Figure 3.** FTIR spectrum of terephthalic acid. The spectrum shows characteristic absorption bands at 3444.7 $cm^{-1}$, 2924 $cm^{-1}$, 2834.8 $cm^{-1}$, 2720.8 $cm^{-1}$, 1600.3 $cm^{-1}$, 1357.3 $cm^{-1}$, 1109.4 $cm^{-1}$, and 777.23 $cm^{-1}$, indicating the presence of various groups.

### *3.3. Field Emission Scanning Electron Microscopy (FESEM)*

The FESEM images of AgONPs (**Figure 4**) provide valuable insights into their morphology and surface characteristics. At a magnification of 50.1kX with a scale bar of 500 nm, the left image reveals numerous nanoparticles with predominantly polygonal shapes. These particles exhibit a degree of agglomeration, indicating that they tend to cluster together. The surface texture appears rough and heterogeneous, suggesting variations in the particle formation process. In the higher magnification image at 94.00kX with a scale bar of 200 nm, the nanoparticles' detailed morphology becomes more evident. The particles are not perfectly spherical; instead, they display irregular shapes with distinct edges and facets. The nanoparticles' porous surfaces are clearly visible. Porosity and surface roughness are crucial for applications in catalysis, medicine, and materials science, as they can influence nanoparticles' reactivity and interactions with other substances.

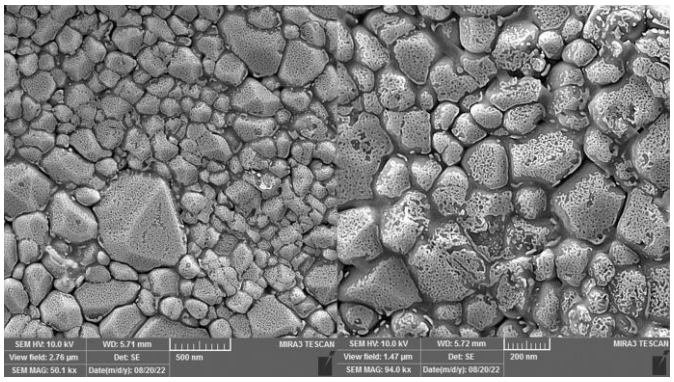


**Figure 4.** FESEM images of AgONPs at magnifications of 50.1kX (left) and 94.0kX (right). The images reveal the morphology and surface characteristics of the nanoparticles, showing polygonal shapes, rough textures, and porous surfaces.

The particle size distribution of AgONPs was analyzed using ImageJ and SPSS frequency analysis from FESEM images. The histogram, overlaid with a bell-shaped curve, indicates that the particle sizes follow a normal distribution (**Figure 5**). The normal distribution curve suggests that most particles were close to the average size, but a considerable range of sizes was present. The analysis revealed a mean particle size of 171.34 nm and a standard deviation of 88.304 nm. This

suggests that although the average nanoparticle size was around 171.34 nm, there was a significant spread, indicating variability among the particles.

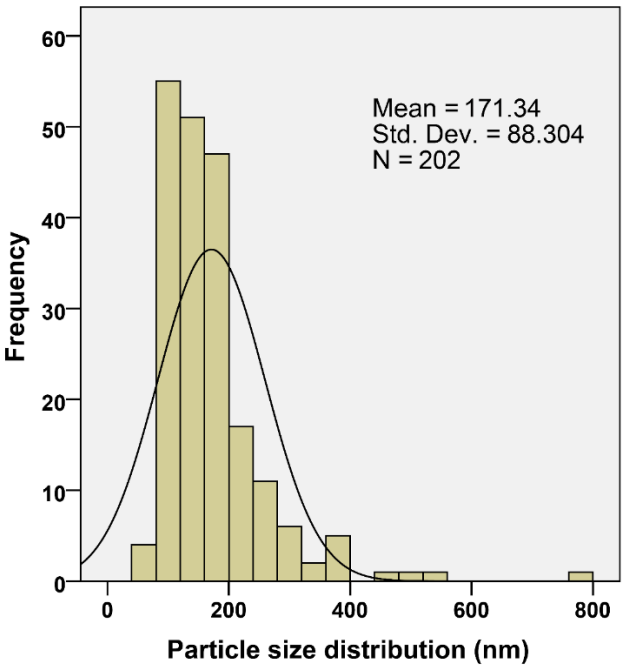


**Figure 5.** Histogram of particle size distribution for AgONPs analyzed using ImageJ and SPSS frequencies analysis from FESEM images. The mean particle size is 171.34 nm, with a standard deviation of 88.304 nm, indicating particle size variability.

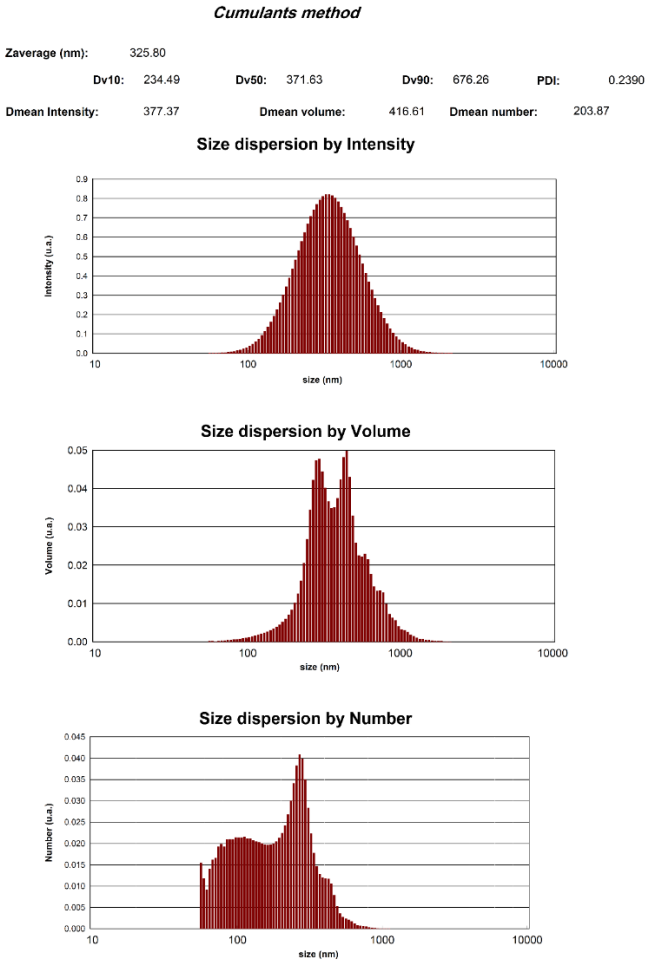


**Figure 6.** DLS results showing the Z-average, PDI, Dv10, Dv50, Dv90, and mean particle sizes based on intensity, volume, and number distributions for AgONPs. Zeta potential results include the mean zeta potential, electrophoretic mobility, and standard deviations, along with experimental parameters such as temperature, electric field, conductivity, dielectric constant, pH, and viscosity.

### *3.4. Dynamic Light Scattering (DLS)*

The DLS results (**Figure 6**) indicated that the AgONPs had an average hydrodynamic diameter (Z-average) of 325.80 nm. The Polydispersity Index (PDI) was 0.2390, suggesting a relatively uniform size distribution and indicating that the nanoparticles were fairly uniform in size. The particle size distribution showed that 10% of the sample's volume consisted of particles smaller than 234.49 nm (Dv10), 50% was smaller than 371.63 nm (Dv50), and 90% was smaller than 676.26 nm (Dv90). The mean particle sizes based on intensity, volume, and number distributions were 377.37 nm, 416.61 nm, and 203.87 nm, respectively, reflecting the different averaging methods. These results provided insights into the size distribution and uniformity of the AgONPs, highlighting the presence of both smaller and larger particles.

The zeta potential measurements revealed that the AgONPs had a mean zeta potential of -19.32 mV, indicating a moderate negative surface charge. This value suggested that the nanoparticles had some degree of stability in suspension, although they might have been prone to aggregation over time. The electrophoretic mobility mean was recorded at -1.55 µm/s/V/cm, with a standard deviation of 0.52, while the standard deviation for the zeta potential was 6.47 mV. The experimental conditions, including a temperature of 26.39 °C, an electric field of 8.23 V/cm, a conductivity of 0.019 mS/cm, a dielectric constant of 77.91, a pH of 6.44, and

a viscosity of 0.8623 mPas, were noted to influence these measurements. These parameters provided a comprehensive understanding of the physical properties and stability of the AgONPs in colloidal solutions. The moderate negative surface charge suggested some degree of electrostatic repulsion, which could help prevent aggregation. However, stability may not be high over time, as higher absolute zeta potentials (above ±30 mV) are typically associated with better stability.

### *3.5. Antibacterial activity of AgONPs*

The smallest average inhibition zone was observed for *E. coli* (9.66 mm), while the largest was for *S. aureus* (17.66 mm). Overall, silver oxide nanoparticles exhibited inhibitory effects against all tested bacterial strains (**Table 2**, **Figure 7**).

The lowest MIC for biosynthesized AgONPs was 75 µg/ml for *S. aureus*, while the highest was 150 µg/ml for *E. coli*. The lowest MBC was also observed for *S. aureus* at 100 µg/ml. No significant difference was found between the MICs of the biosynthesized AgONPs and chloramphenicol for both Gram-positive and Gram-negative strains ($p < 0.5$). The MBC/MIC ratio indicated that the biosynthesized AgONPs exhibit bactericidal activity against both Gram-positive and Gram-negative bacteria (**Table 2**).

### *3.7. Antibiofilm activity of AgONPs*

#### *3.7.1 Investigation of biofilm formation*

The biofilm formation of *E. coli* ATCC 25922, *P. aeruginosa* ATCC 9027, *B. subtilis* PTCC 1365, and *S. aureus* ATCC 25923 was evaluated, and the results were measured at 492 nm using an ELISA reader. After obtaining the $OD_{492}$ values, biofilm formation was assessed using the cut-off method. Phenotypic analysis with microtiter plates revealed that all tested bacterial strains formed strong biofilms (**Table 3**).

**Table 2:** Diameter of the non-growth zone (mm), MIC, MBC, and MBC/MIC ratios of AgONPs against 4 ATCC bacteria.

| Test | Material | *E. coli* ATCC 25922 | *P. aeruginosa* ATCC 9027 | *B. subtilis* PTCC 1365 | *S. aureus* ATCC 25923 |
|---|---|---|---|---|---|
| **Disk diffusion** | AgONPs (500 µg/ml) | 9.66±0.1 mm | 13.33±0.1 mm | 11.33±0.1 mm | 17.66±0.1 mm |
| | Gentamicin (10 µg) [Control] | 20.66±0.1 mm | 21.33±0.1 mm | 21±00 mm | 27.66±0.2 mm |
| **MIC** | AgONPs | 150 ±00 µg/ml | 125±00 µg/ml | 125±00 µg/ml | 75±00 µg/ml |
| | Chloramphenicol [Control] | 25±00 µg/ml | 25±00 µg/ml | 25±00 µg/ml | 25±00 µg/ml |
| **MBC** | AgONPs | 175±00 µg/ml | 175±00 µg/ml | 150±00 µg/ml | 100±00 µg/ml |
| | Chloramphenicol [Control] | 25±00 µg/ml | 25±00 µg/ml | 25±00 µg/ml | 25±00 µg/ml |
| **MBC/MIC ratio** | AgONPs | 1.16 (+) | 1.4 (+) | 1.2 (+) | 1.33 (+) |
| | Chloramphenicol [Control] | 1 (+) | 1 (+) | 1 (+) | 1 (+) |

(+): Bactericidal

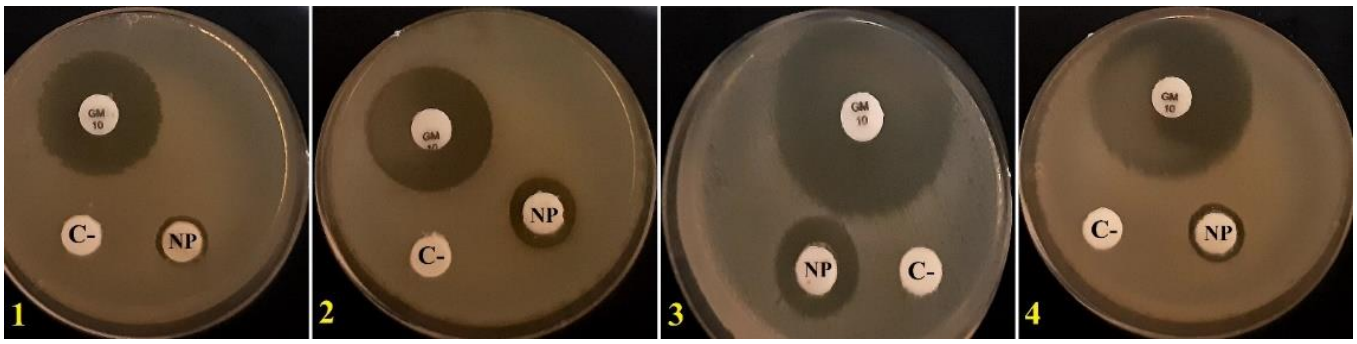


**Figure 7.** Antibacterial activity of AgONPs using the disk diffusion method. **(**NP: Silver oxide nanoparticles; C-: Negative control; GM: Gentamicin; 1: *Escherichia coli*; 2: *Pseudomonas aeruginosa*; 3: *Staphylococcus aureus*; 4: *Bacillus subtilis*)

**Table 3.** The optical density ($OD_{492}$) of bacterial strains was measured after 48 hours of biofilm formation.

| **Bacterial strains and control** | *E. coli* ATCC 25922 | *P. aeruginosa* ATCC 9027 | *B. subtilis* PTCC 1365 | *S. aureus* ATCC 25923 | Control |
|---|---|---|---|---|---|
| **mean±standard deviation** | 1.832±0.0008 | 2.528±0.0022 | 1.716±0.0011 | 1.932±0.0007 | 0.296 |

### *3.7.2 Determining the lowest concentration of AgONPs on inhibition of bacterial biofilm formation*

Biofilm formation was investigated in the presence of various concentrations of AgONPs. As displayed in **Figure 8**, biofilm formation decreased as the concentration of AgONPs increased. This was reflected by a reduction in optical absorbance, indicating that higher nanoparticle concentrations inhibit biofilm formation more effectively. At certain concentrations, complete inhibition of biofilm formation was observed, and a slight increase in absorbance was noted, attributed to the presence of nanoparticles rather than biofilm growth, compared to the control.

Notably, *S. aureus* biofilm formation was inhibited entirely at a lower concentration (100 µg/mL) than that of other bacterial strains. Overall, the anti-biofilm effect of AgONPs was more pronounced against Gram-positive strains than Gram-negative strains, with lower concentrations effectively inhibiting biofilm formation in Gram-positive bacteria.

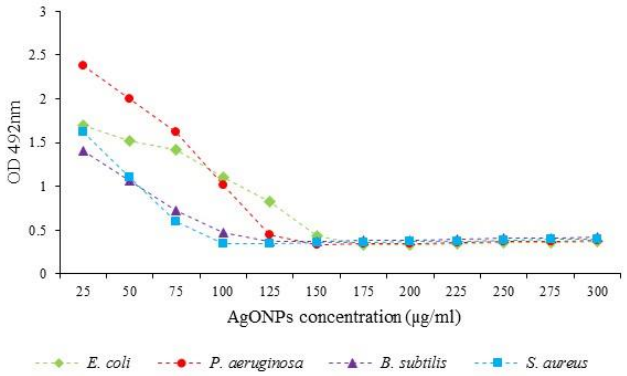


**Fig. 8.** The effect of AgONPs on the inhibition of bacterial biofilm formation

### *3.7.3 Determining the lowest concentration of AgONPs in removing the formed biofilm*

**Figure 9** shows that biofilm removal increased with higher AgONP concentrations. At the minimum concentration that effectively removed the biofilm, absorbance increased only slightly, likely due to the presence of nanoparticles compared to the control.

The results indicate that AgONPs were more effective at removing biofilm formed by Gram-positive strains than by Gram-negative strains. Additionally, AgONPs removed a higher percentage of the biofilm produced by S. aureus than the biofilm formed by other bacterial species at the same concentrations.

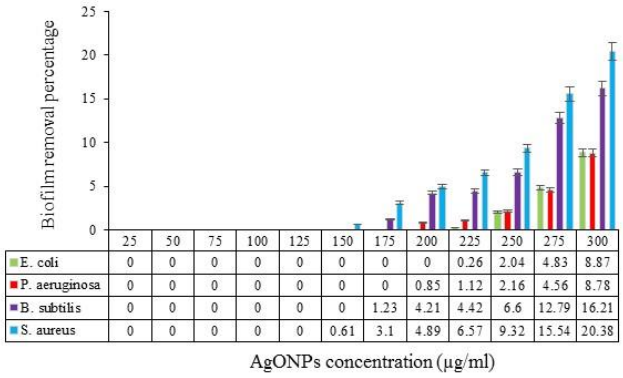


| | 25 | 50 | 75 | 100 | 125 | 150 | 175 | 200 | 225 | 250 | 275 | 300 |
|---|---|---|---|---|---|---|---|---|---|---|---|---|
| E. coli | 0 | 0 | 0 | 0 | 0 | 0 | 0 | 0 | 0.26 | 2.04 | 4.83 | 8.87 |
| P. aeruginosa | 0 | 0 | 0 | 0 | 0 | 0 | 0 | 0.85 | 1.12 | 2.16 | 4.56 | 8.78 |
| B. subtilis | 0 | 0 | 0 | 0 | 0 | 0 | 1.23 | 4.21 | 4.42 | 6.6 | 12.79 | 16.21 |
| S. aureus | 0 | 0 | 0 | 0 | 0 | 0.61 | 3.1 | 4.89 | 6.57 | 9.32 | 15.54 | 20.38 |

**Fig. 9.** The removal percentage of the biofilm formed in the presence of different concentrations of AgONPs.

## 4. Conclusion

AgONPs have shown considerable promise in cancer therapy due to their unique properties, including high surface area, enhanced reactivity, and the ability to induce oxidative stress in cancer cells. The synthesis of AgONPs using terephthalic acid and calcination at 600°C provides a controlled method to produce nanoparticles with specific characteristics. This study aimed to synthesize and characterize AgONPs, followed by an evaluation of their cytotoxicity against cancer cells. The synthesis process involved preparing a silver-terephthalate precursor, which was then calcined to form AgONPs. The nanoparticles were fully characterized. XRD analysis confirmed the formation of cubic AgONPs with a space group of F-43m and lattice parameters of a = 4.8160 Å. FESEM images revealed that the

nanoparticles had a mean size of 171.34 nm, with a standard deviation of 88.304 nm, indicating a relatively uniform size distribution. The FTIR spectrum showed characteristic absorption bands corresponding to Ag-O bonds and various functional groups, confirming the presence of silver oxide and residual organic compounds from the synthesis process. DLS and zeta potential analyses provided further insights into the size distribution and surface charge of the nanoparticles, with a moderate negative zeta potential indicating some degree of suspension stability. The antimicrobial activity of AgONPs is strong, inhibiting gram-negative and gram-positive bacteria. These findings contribute to the growing body of knowledge on the application of AgONPs in cancer therapy. The findings of this study reinforce the potential of AgONPs as effective antibacterial and antibiofilm agents. Their ability to inhibit the growth of various bacterial strains and disrupt biofilm formation positions AgONPs as promising candidates for addressing critical challenges in healthcare and industry. Continued research will be essential to fully harness their capabilities and ensure safe and effective application in real-world settings.

### Acknowledgment

None.

### Conflict of interest

There is no conflict of interest to declare.

### Data availability

All of the data are included in the article.

### Authors Contributions

MTAA, ATAA, MM, AE and EY developed the theoretical formalism, performed the analytic calculations and performed the numerical simulations. All of the authors contributed to the final version of the manuscript. AE supervised the project.

### Funding

None.

### Using artificial intelligence chatbots

There was no use of artificial intelligence in the making of this article.

## References

1. Taghavizadeh Yazdi ME, Qayoomian M, Beigoli S, Boskabady MH. Recent advances in nanoparticle applications in respiratory disorders: A Review. Frontiers in Pharmacology. 2023;14:1059343.
2. Eslamieh-Ei FM, Sharifimoghaddammood N, Poustchi Tousi SA, Basharkhah S, Mottaghipisheh J, Es-Haghi A, et al. Synthesis and its characterisation of selenium/silver/chitosan and cellular toxicity against liver carcinoma cells studies. Natural Product Research. 2023:1-9.
3. Hashemzadeh V, Hashemzadeh A, Mohebbati R, Arefi RG, Yazdi MET. Fabrication and characterization of gold nanoparticles using alginate: In vitro and in vivo assessment of its administration effects with swimming exercise on diabetic rats. Open Life Sciences. 2024;19(1):20220869.
4. Shahifar A, Bagheri H, Namnabat S. Synthesis and Evaluation of a Polycaprolactone-methoxy-Polyethyleneglycol Copolymer Nano-system for Curcumin and Tacrolimus Release: Drug Delivery Nano-system. Iranian Journal of Pharmaceutical Sciences. 2023;19(4):304-13.
5. Ghasemzadeh Rahbardar M, Taghavizadeh Yazdi ME, Beigoli S, Amin H, Boskabady MH. Exploring the role of curcumin, nanocurcumin, and a PPAR agonist in preventing paraquat-induced systemic inflammation and oxidative stress in rats. Iranian Journal of Basic Medical Sciences. 2025.
6. Hashemzadeh A, abdulrazzaq Al-hakeem M, Hsu C-Y, Tomar P, Hjazi A, Kadhum WR, et al. Polyphenol-Functionalized Metal-Organic Frameworks: A Strategic Platform for Advanced Cancer Drug Delivery and Synergistic Therapy. Materials Research Bulletin. 2025:113778.
7. Gudkov SV, Serov DA, Astashev ME, Semenova AA, Lisitsyn AB. Ag2O Nanoparticles as a Candidate for Antimicrobial Compounds of the New Generation. Pharmaceuticals. 2022;15(8).
8. Yazdi MET, Amiri MS, Akbari S, Sharifalhoseini M, Nourbakhsh F, Mashreghi M, et al. Green synthesis of silver nanoparticles using helichrysum graveolens for biomedical applications and wastewater treatment. BioNanoScience. 2020;10(4):1121-7.
9. Yazdi MET, Amiri MS, Hosseini HA, Oskuee RK, Mosawee H, Pakravanan K, et al. Plant-based synthesis of silver nanoparticles in Handelia trichophylla and their biological activities. Bulletin of Materials Science. 2019;42(4):155.
10. Zarei M, Karimi E, Oskoueian E, Es-Haghi A, Yazdi MET. Comparative study on the biological effects of sodium citrate-based and apigenin-based synthesized silver nanoparticles. Nutrition and Cancer. 2021;73(8):1511-9.
11. Moges-Tsegaye M, Kumar M, Pandey SP, Fentie-Tasew M, Yadav P, Chouhan G. Characterization and Antibacterial Activity of Plant-Mediated Silver Oxide Nanoparticles. Macromolecular Symposia. 2023;407(1).
12. Yazdi MET, Nourbakhsh F, Mashreghi M, Mousavi SH. Ultrasound-based synthesis of ZnO· Ag 2 O 3

nanocomposite: characterization and evaluation of its antimicrobial and anticancer properties. Research on Chemical Intermediates. 2021;47(3):1285-96.
13. Rivera-Mendoza D, Quiñones B, Huerta-Saquero A, Castro-Longoria E. Antimicrobial Activity of Green Synthesized Silver and Copper Oxide Nanoparticles against the Foodborne Pathogen Campylobacter jejuni. Antibiotics. 2024;13(7):650.
14. Yazdi MET, Khara J, Sadeghnia HR, Bahabadi SE, Darroudi M. Biosynthesis, characterization, and antibacterial activity of silver nanoparticles using Rheum turkestanicum shoots extract. Research on Chemical Intermediates. 2018;44(2):1325-34.
15. Yazdi MET, Modarres M, Amiri MS, Darroudi M. Phyto-synthesis of silver nanoparticles using aerial extract of Salvia leriifolia Benth and evaluation of their antibacterial and photo-catalytic properties. Research on Chemical Intermediates. 2019;45(3):1105-16.
16. Hamidi A, Yazdi MET, Amiri MS, Hosseini HA, Darroudi M. Biological synthesis of silver nanoparticles in Tribulus terrestris L. extract and evaluation of their photocatalyst, antibacterial, and cytotoxicity effects. Research on Chemical Intermediates. 2019;45(5):2915-25.
17. Vellingiri MM, Ashwin JKM, Soundari AJPG, Sathiskumar S, Priyadharshini U, Paramasivam D, et al. Mycofabrication of AgONPs derived from Aspergillus terreus FC36AY1 and its potent antimicrobial, antioxidant, and anti-angiogenesis activities. Molecular Biology Reports. 2021;48(12):7933-46.
18. Ravi L, Chocalingum R, Menta V, Krishnan K. Marine actinomycetes derived pyrrolo compounds mediated green synthesis of AgO and Ag2O3 nanoparticles and its antidermatophytic activity. Nanoscience and Nanotechnology - Asia. 2020;10(6):868-75.
19. Mathimaran A, Pandian CJ, Sappanimuthu P, Kirshnakumar H, Amala M, Veerapandiyan M, et al. Synthesis of multifunctional silver oxide, zinc oxide, copper oxide and gold nanoparticles for enhanced antibacterial activity against ESKAPE pathogens and antioxidant, anticancer activities using Momordica cymbalaria seed extract. Materials Today Communications. 2024;39:108838.
20. Ullah Z, Iqbal J, Gul F, Abbasi BA, Kanwal S, Elsadek MF, et al. Biogenic synthesis, characterization, and in vitro biological investigation of silver oxide nanoparticles (AgONPs) using Rhynchosia capitata. Scientific Reports. 2024;14(1).
21. Zhang Y, Tang Y, Liao Q, Qian Y, Zhu L, Yu D-G, et al. Silver oxide decorated urchin-like microporous organic polymer composites as versatile antibacterial organic coating materials. Journal of Materials Chemistry B. 2024;12(8):2054-69.
22. Mousavi-Kouhi SM, Beyk-Khormizi A, Amiri MS, Mashreghi M, Yazdi MET. Silver-zinc oxide nanocomposite: From synthesis to antimicrobial and anticancer properties. Ceramics International. 2021;47(15):21490-7.
23. Rahimi E, Asefi F, Afzalinia A, Khezri S, Zare-Zardini H, Ghorani-Azam A, et al. Chitosan coated copper/silver oxide nanoparticles as carriers of breast anticancer drug: Cyclin D1/P53 expressions and cytotoxicity studies. Inorganic Chemistry Communications. 2023:111581.
24. Nateq Golestan M, Abbasi MR, Rakhshandeh H, Taghavizadeh Yazdi ME. Facile fabrication and characterization of silver nanoparticles by sunn pest (Eurygaster integriceps puton) damaged wheat and evaluation of its antibacterial and cellular toxicity toward liver cancer cell lines. Studies in Medical Sciences. 2023;34(10):586-97.
25. Ahmadinejad F, Møller SG, Hashemzadeh-Chaleshtori M, Bidkhori G, Jami MS. Molecular mechanisms behind free radical scavengers function against oxidative stress. Antioxidants. 2017;6(3).
26. Hong Y, Zeng J, Wang X, Drlica K, Zhao X. Post-stress bacterial cell death mediated by reactive oxygen species. Proceedings of the National Academy of Sciences. 2019;116(20):10064-71.
27. Ahmadi R, Es-haghi A, Zare-Zardini H, Taghavizadeh Yazdi ME. Nickel oxide nanoparticles synthesized by Rose hip extract exert cytotoxicity against the HT-29 colon cancer cell line through the caspase-3/caspase-9/Bax pathway. Emergent Materials. 2023;6(6):1877-88.
28. Beigoli S, Hajizadeh AA, Yazdi MET, Zarei H, Vafaee F, Boskabady MH. The brain and systemic oxidative stress and memory changes induced by inhaled paraquat in rat improved by Crocus sativus. Legal Medicine. 2024:102525.
29. Yazdi MET, Darroudi M, Amiri MS, Hosseini HA, Nourbakhsh F, Mashreghi M, et al. Anticancer, antimicrobial, and dye degradation activity of biosynthesised silver nanoparticle using Artemisia kopetdaghensis. Micro & Nano Letters. 2020;15(14):1046-50.
30. Bagherian MS, Zargham P, Zarharan H, Bakhtiari M, Mortezaee Ghariyeh Ali N, Yousefi E, et al. Antimicrobial and antibiofilm properties of selenium-chitosan-loaded salicylic acid nanoparticles for the removal of emerging contaminants from bacterial pathogens. World Journal of Microbiology and Biotechnology. 2024;40(3):86.
31. Es-Haghi A, Amiri MS, Taghavizadeh Yazdi ME. Ferula latisecta gels for synthesis of zinc/silver binary nanoparticles: antibacterial effects against gram-negative and gram-positive bacteria and physicochemical characteristics. BMC biotechnology. 2024;24(1):51.
32. Patel JB. Performance standards for antimicrobial susceptibility testing: twenty-fourth informational supplement. (No Title). 2014.
33. Mogana R, Adhikari A, Tzar M, Ramliza R, Wiart C. Antibacterial activities of the extracts, fractions and isolated compounds from Canarium patentinervium Miq. against bacterial clinical isolates. BMC complementary medicine and therapies. 2020;20(1):1-11.